FULL PAPER

Dalton
www.rsc.org/dalton

A new series of layered transition metal oxalates: hydrothermal synthesis, structural and magnetic studies

Daniel J. Price,† Annie K. Powell‡ and Paul T. Wood§
School of Chemical Sciences, University of East Anglia, Norwich, UK NR4 7TJ

Received 11th February 2003, Accepted 1st May 2003
First published as an Advance Article on the web 20th May 2003

The hydrothermal synthesis and crystallographic study of a new family of isostructural transition metal oxalate compounds, $Ba_2M_2(ox)_3Cl_2(H_2O)_4$ (M = Mn(II) (**1**), Fe(II) (**2**) or Co(II) (**3**)) is reported. The crystal structure has *C*2/*c* symmetry and contains two types of oxalate. These dianionic ligands bridge the transition metal ions in two different modes, which together form a 2-D net comprised of linked chains of transition metal ions. The iron derivative shows strong evidence of antiferromagnetic coupling interactions and significant short-range magnetic order at low temperatures but there is no evidence of long-range ordering above 2 K. Attempts to fit the observed magnetic susceptibility to several approximate models is reviewed. The Co derivative also shows antiferromagnetic coupling and additionally appears to have a magnetic phase transition at about 11(1) K.

Introduction

There are two good reasons why oxalate coordination networks are subject to much interest. Firstly from a structural perspective the dominance of the η^4-chelating coordination mode and the related bis-η^4-chelate bridging mode provides a degree of structural predictability. In theory a large variety of network structures could be formed. Finding which structure types can be obtained in reality and how we can control the formation of one network in preference to another is of great significance. Work by the groups of Rao[1] and Cheetham[2] has been successful in extending the range of known structure types.

A second point of interest derives from the fact that the oxalate anion can mediate a reasonable magnetic exchange between bridged paramagnetic ions.[3] Since the magnetic behaviour of exchange-coupled systems depends wholly on the network structure; its dimensionality and its topology, the ability to form predictable well-defined structures is of the utmost importance. For these reasons transition metal oxalates have long been of considerable interest to magnetochemists.

While simple transition metal oxalates often adopt a 1-D chain structure, typified by the naturally occurring iron mineral humboldtine;[4] $Fe(ox)(H_2O)_2$, it has been shown that additional non-coordinating cations A^{n+}, can stabilize two-dimensional[5] and three-dimensional[6] anionic networks with typical compositions $A_x[MM'(ox)_3]$.

Experimental

IR spectra were recorded as KBr pellets on a Nicollet 410 Impact FTIR spectrometer, while electronic spectra were obtained with a diffuse reflectance adaptation on a Perkin Elmer UV-VIS-NIR Lambda 19 spectrometer, from samples in a $BaSO_4$ matrix. Elemental analysis was performed by the UEA Microanalysis Service. Static magnetic susceptibility measurements were measured between 2 and 300 K as field-cooled experiments with H = 100 G, on a Quantum Design MPMS SQUID magnetometer. Measurements were made on powdered samples, held in an eicosane matrix to prevent reorientation in the applied field. A correction for the diamagnetic contribution to the susceptibility was made based upon Pascal's constants;[7] χ_{dia} for **2** and **3** was calculated as 127×10^{-6} cm^3 mol^{-1}.

Synthesis

While **1**, **2** and **3** can be synthesised under a range of conditions, a large excess of $BaCl_2$ is an essential component. The synthesis reported here are optimised conditions minimising the extent of contamination by other insoluble oxalate phases. In the case of **2** and **3** the products are formed at about 99% phase purity. A phase pure sample of **1** has never been obtained, even after an exhaustive and systematic search of the reaction phase space. The reported method gives the product at about 60% purity, with a number of different manganese oxalate phases as contaminants.

$Ba_2[Mn_2Cl_2(C_2O_4)_3]\cdot 4H_2O$ (1). A mixture of manganese(II) chloride tetrahydrate (197 mg, 1.0 mmol), sodium oxalate (166 mg, 1.2 mmol), barium chloride dihydrate (1.957 g, 8.0 mmol) and distilled water (10 ml) was placed in a 23 ml Teflon lined autoclave and heated to 225 °C for 2 h. The reaction mixture was then cooled at 0.1 °C min^{-1} back to room temperature. The solid products were collected by filtration and dried in air. The major product formed colourless diamond shaped microcrystalline platelets. Optical microscopy showed contamination by a number of crystals with different morphology (Found: C, 9.90; H, 0.86; Cl, 4.80. $Ba_2Mn_2Cl_2C_6O_{16}H_8$ requires; C, 9.10; H, 1.02; Cl, 8.96%).

$Ba_2[Fe_2Cl_2(C_2O_4)_3]\cdot 4H_2O$ (2). As for **1**, but with the following quantities: iron(II) chloride tetrahydrate (0.199 g, 1.00 mmol), sodium oxalate (0.197 g, 1.47 mmol), barium chloride dihydrate (2.415 g, 9.90 mmol) and distilled water (10 ml). The pure crystalline product was obtained as orange platelets (yield: 466 mg, 80%) (Found: C, 9.15; H, 0.86; Cl, 9.08. $Ba_2Fe_2Cl_2C_6O_{16}H_8$ requires; C, 9.08; H, 1.02; Cl, 8.94%). λ_{max}/nm ($BaSO_4$) 350 (relative absorbance 0.39), 982 (0.14) and 1285 (0.158) both $^5T_{2g} \longrightarrow {}^5E_g$ split by Jahn–Teller effects; ν_{max}/cm^{-1} (KBr) 3605m, 3478s, 3445s, 3350s, 1678s, 1640s, 1601s, 1466w, 1335m, 1305m, 905vw, 854vw, 791m, 748w, 644w, 614w, 516w and 470m.

$Ba_2[Co_2Cl_2(C_2O_4)_3]\cdot 4H_2O$ (3). As for **1**, but with the following quantities: cobalt(II) chloride hexahydrate (201 mg, 0.85 mmol), sodium oxalate (203 mg, 1.51 mmol), barium chloride dihydrate (4.46 g, 18.3 mmol) and distilled water (7 ml). The product was obtained pure as purple platelets (yield: 309 mg, 91.3%) (Found: C, 9.05; H, 0.77; Cl, 9.08. $Ba_2Co_2Cl_2C_6O_{16}H_8$ requires; C, 9.01; H, 1.01; Cl, 8.87%). λ_{max}/nm ($BaSO_4$) 305 (relative

† Present address: Department of Chemistry, University of Southampton, Highfield, Southampton, UK, SO17 1BJ. E-mail Daniel.Price@soton.ac.uk
‡ Present address: Institut für Anorganische Chemie der Universität, D-76128 Karlsruhe, Germany.
§ Present address: Universtiy Chemistry Laboratory, Lensfield Road, Cambridge, UK, CB2 1EW.

DOI: 10.1039/b301658g

Table 1 Crystallographic details for **1**, **2** and **3**

Compound	**1** (Mn)	**2** (Fe)	**3** (Co)
Formula	$Ba_4Mn_4Cl_4C_{12}H_{16}O_{32}$	$Ba_4Fe_4Cl_4C_{12}H_{16}O_{32}$	$Ba_4Co_4Cl_4C_{12}H_{16}O_{32}$
Formula weight	1583.18	1586.82	1599.14
Crystal system	Monoclinic	Monoclinic	Monoclinic
Space group	*C*2/*c*	*C*2/*c*	*C*2/*c*
a/Å	22.916(5)	22.789(5)	22.675(5)
b/Å	8.248(2)	8.297(2)	8.230(2)
c/Å	9.904(2)	9.849(2)	9.757(2)
β/°	99.53(3)	99.90(3)	100.00(3)
V/Å^3	1846.1(6)	1835.3(6)	1793.1(6)
Z	2	2	2
D_c/Mg m^{-3}	2.848	2.871	2.962
Reflections collected	6319	2724	7235
Independent reflections	2188	1481	2195
R_{int}	0.1098	0.0280	0.0449
$R1$ $I > 2\sigma(I)$ (all data)	0.0362 (0.0380)	0.0191 (0.0236)	0.0305 (0.0377)
$wR2$ $I > 2\sigma(I)$ (all data)	0.0867 (0.0875)	0.0495 (0.0839)	0.0760 (0.0784)

absorbance 0.29), 540 (0.30) $^4T_{1g}(F) \longrightarrow {}^4T_{1g}(P)$, 688 (0.189) $\longrightarrow$ $^4A_{2g}(F)$ and 1350 (0.21) $\longrightarrow$ $^4T_{2g}(F)$; ν_{max}/cm^{-1} (KBr) 3595m, 3480s, 3448s, 3353s, 1675s, 1636s, 1598s, 1470w, 1336m, 1306m, 906vw, 854vw, 793m, 751w, 649w, 568w and 471m.

X-Ray structure determination

For all three samples room-temperature data was collected on a Rigaku RAxisII image plate diffractometer as a series of 45 $\Delta\varphi$ oscillation photographs, with $\Delta\varphi = 5°$. Graphite monochromated Mo-Kα radiation ($\lambda = 0.71073$ Å) was used from a rotating anode source. The data were processed using the programs DENZO and SCALEPACK.[8] No absorption corrections were applied. The structures were solved by direct methods and refined[9] by a full-matrix least squares on F^2. All non-hydrogen atoms were refined anisotropically. Selected crystallographic details can be found in Table 1.

CCDC reference numbers 203681–203683.

See http://www.rsc.org/suppdata/dt/b3/b301658g/ for crystallographic data in CIF or other electronic format.

Results and discussion

Synthetic considerations

The compounds $Ba_2M_2(ox)_3Cl_2(H_2O)_4$ (M = Mn, **1**; Fe, **2**; Co, **3**) are synthesised by hydrothermal reactions containing a mixture of barium chloride, the transition metal chloride, sodium oxalate and water [in approximately 30 : 2 : 3 : 800 molar ratios]. The suspension is heated under autogenous pressure to 225 °C and allowed to cool back to room temperature slowly, whereupon crystals of the product are formed. It appears that **1**, **2** and **3** can only be formed under conditions where there is a higher proportion of barium chloride in the starting solution than in the product. Upon standing in distilled water crystals of **1**, **2** and **3** are transformed into a fine white precipitate of barium oxalate. These compounds can be formulated either as Ba(ox)·$BaCl_2$·2M(ox)·4H_2O or equivalently 2Ba(ox)·MCl_2·M(ox)·4H_2O, as such they can be classified as *hydrated triple salts* that are decomposed by water.[10] In principle these phases can be formed from solutions of just these three components, crystallisation occurring as the saturation curve is crossed. For three components, as in this case, the saturation curve forms a surface covering a range of different Ba(ox) : $BaCl_2$: M(ox) compositions. Solutions with the 1 : 1 : 2 [Ba(ox)–$BaCl_2$–M(ox)] composition lie outside the region covered by the saturation curve of these complex triple salts, and thus crystals of the product can never be grown from such a solution with the same composition as the solid. The excess $BaCl_2$ required for crystallisation implies a relatively high barium or chloride chemical potential is needed before this phase can be produced. The observed phase is only thermodynamically stable with respect to barium oxalate and transition metal oxalates under very high concentrations of $BaCl_2$. It is interesting that no similar materials were formed in analogous reactions with $BaBr_2$.

The phase was initially identified in an investigation of the $BaCl_2$–Na(ox)–$FeCl_3$ hydrothermal reaction phase diagram, where an *in situ* coupled reduction of the iron(III) and oxidation of the ox^{2-} ions is required. Although our optimised synthesis starts with the M(II) salts, for a large region of the 'synthetic phase space' the products are contaminated with other insoluble oxalates and small quantities of transition metal oxides. The oxide formation is the result of hydrolysis, and under these synthetic conditions the oxides are the thermodynamically most stable phases. This is consistent with the observation that the extent of oxide formation is in proportion to the reaction time and temperature. For **2** and **3** the best synthesis affords the product at about 99% purity and the impurity phases can be manually removed. This purification is made easier by the characteristic colours of these products (Fe–orange, Co–purple). The clean synthesis of **1** is more difficult, and our method produces at best a sample about 60% phase pure. Purification of this material by manual crystal selection is not possible as the product and impurities are similarly sized, insoluble colourless crystals with similar densities. The lack of a macroscopically pure sample of **1** has limited its bulk characterisation.

Crystal structures

The compounds are isomorphous and isostructural, crystallising as diamond shaped platelets in the monoclinic space group *C*2/*c*. Crystallographic details are given in Table 1. The asymmetric unit contains one transition metal ion in a distorted octahedral environment (Fig. 1). The metal is coordinated by three oxalates and a chloride ion. Two oxalate ions are chelating in a *cis*-geometry and thus the metal centres are chiral, however the centrosymmetric space group ensures equal numbers of Δ and Λ enantiomeric centres throughout the crystal. One of the oxalates has an inversion centre at its C–C centroid and so bridges two metals in a symmetric bis-chelating mode (Fig. 2(a)). This can be considered to create an anionic dimeric unit $[Cl(ox)M(ox)M(ox)Cl]^{4-}$ from which the network is built. Here each metal has opposite chirality. The second oxalate chelates one metal ion and bridges another in a unidentate fashion (Fig. 2(a)). The metal–oxalate network formed by these two bridging modes is a puckered 2-D sheet, shown schematically in Fig. 2(b). There are strong similarities with the previously reported compounds $Na_2Co_2(ox)_3(H_2O)_2$[11] and $Cs_2Mn_2(ox)_3(H_2O)_3$,[12] where a similar Δ,Λ-[(ox)M(ox)M(ox)] dimer unit forms the basis of an extended network structure. These dimers link up with the same bridging modes as with those compounds presented here, but form a ladder structure (Fig. 2(c)). Which of these two network motifs is formed simply depends upon the

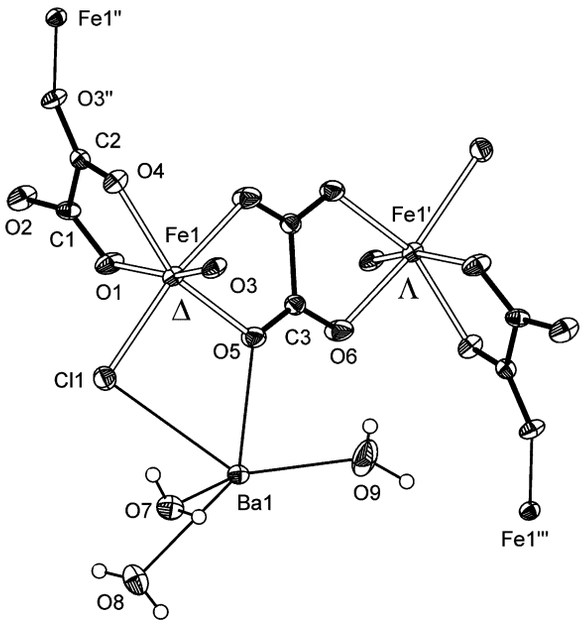

Fig. 1 The asymmetric unit of **2** and selected symmetry equivalent atoms. This shows the dimeric structural unit $[Cl(ox)M(ox)M(ox)Cl]^{4-}$ and how the two types of oxalate present bridge the metal ions. Thermal ellipsoids are at the 50% probability level.

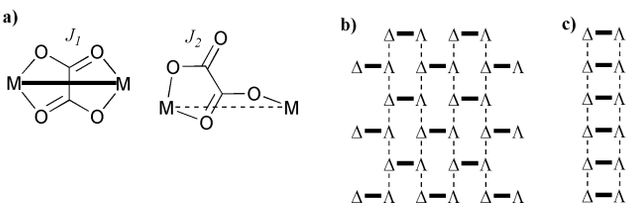

Fig. 2 The oxalate bridging modes and the network structures they form. In (a) the thick solid lines represent the symmetric μ-oxalato bridged Δ,Λ-dimer and the dashed line shows the asymmetric oxalate bridging. Two structures are easily formed: (b) the 2-D sheet formed by the present series of compounds and (c) the 1-D ladder formed in the related compound [11] $Na_2Co_2(ox)_3(H_2O)_2$.

relative chirality of adjacent metal ions. A packing diagram showing the corrugated layer structure of the network is shown in Fig. 3.

Between these sheets are a layer of barium cations and water of crystallisation. The bariums sit partly in the corrugations formed by the transition metal–oxalate net and are coordinated by one chloride, three waters (one of which is disordered over two nearby sites) and six oxygen atoms from four oxalate anions. Ba–O bond lengths are in the range 2.76(3)–3.132(3) Å.

There are three crystallographically independent water molecules in the structure. Two lie midway between metal–oxalate layers and bridge barium cations in a μ_2-fashion. Each proton on these waters forms a hydrogen bond to the chloride ions forming a cyclic $R_4^2(8)$ motif.[13] The third water molecule also coordinates to the barium, but resides in the cleft formed by the corrugated metal–oxalate sheet. This water is disordered over two sites and forms an extensive 2-D hydrogen bonded network that interpenetrates the metal–oxalate layer.

The transition metal coordination sphere is a distorted octahedron (Table 2). This distortion is a consequence of steric factors such as the rigid geometry of the oxalato ion and crystal packing forces. The degree of distortion from an ideal octahedral geometry increases from Co^{2+}, Fe^{2+} to Mn^{2+}. This correlates well with the different electronic configurations of these ions and their CFSE. Some angular changes are much more pronounced than others. For example there are large changes in the O1–M–O5 and O4–M–Cl1 angles while the O3–M–O5 and O1–M–Cl1 angles seem to hardly change at all. Care must be taken in trying to understand the significance of these angular changes as many of these quantities are correlated such as the O1–M–O4 angle and the metal ion size. The average M–O bond lengths show the expected general decrease with Mn > Fe > Co, but bond lengths also reveal interesting distortions, with *trans*-pairs of M–O bonds tending to become equal in length as the series progresses from Mn (**1**) to Co (**3**).

Table 2 Selected bond lengths (Å), bond angles (°) and averages, revealing the changing nature of the bonding in the transition metal coordination sphere

Compound (M)	**1** (Mn)	**2** (Fe)	**3** (Co)
Bond length			
M–O1	2.149(3)	2.118(2)	2.079(3)
M–O3	2.158(2)	2.122(2)	2.077(3)
M–O5	2.184(3)	2.143(2)	2.120(3)
M–O4	2.220(2)	2.173(2)	2.126(3)
M–O6′	2.266(3)	2.219(2)	2.179(3)
M–Cl1	2.4970(12)	2.4679(9)	2.4318(13)
Mean M–O	2.1954(48)	2.1550(42)	2.1162(42)
Bond angle			
O1–M–O3	159.91(10)	162.40(7)	163.88(10)
O4–M–O5	154.07(10)	156.22(8)	157.99(11)
O6′–M–Cl1	168.73(8)	170.06(6)	170.91(10)
Mean deviation from 180°			
	19.10	17.11	15.74

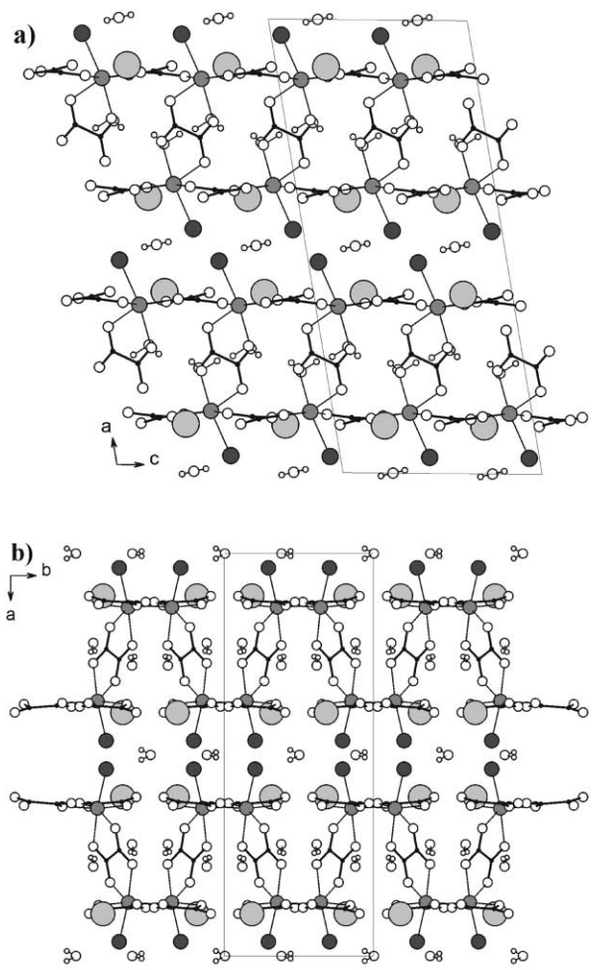

Fig. 3 Packing diagrams: transition metal (mid grey), chlorine (dark grey), barium (light grey). View (a) shows transition metal–oxalate sheets and the interlayer positions of the barium counter ions viewed along the [010] axis and (b) shows the puckered nature of the sheets along the [001] axis.

Magnetic studies

Magnetic susceptibility studies have been performed on **2** and **3** (impure samples have frustrated useful studies on **1**). The magnetic susceptibility of the iron compound **2** (Fig. 4(a)) increases on cooling reaching a broad maximum at 14(±0.4) K with $\chi_{max} = 0.1054(1)$ cm^3 mol^{-1} (all magnetic quantities are per mole of M(II) ions, not per formula unit). Plotting as reciprocal susceptibility *vs.* temperature (Fig. 5(a)) shows that above ~50 K the sample obeys a Curie–Weiss law, with $C = 3.59(1)$ cm^3 K mol^{-1} and $\theta = -4.5(5)$ K. The large high temperature effective moment of 5.36 μ_B compared to the spin-only value of $S = 2$ (4.90 μ_B) can be attributed to the orbital contribution from the $^5T_{2g}$ ground term.

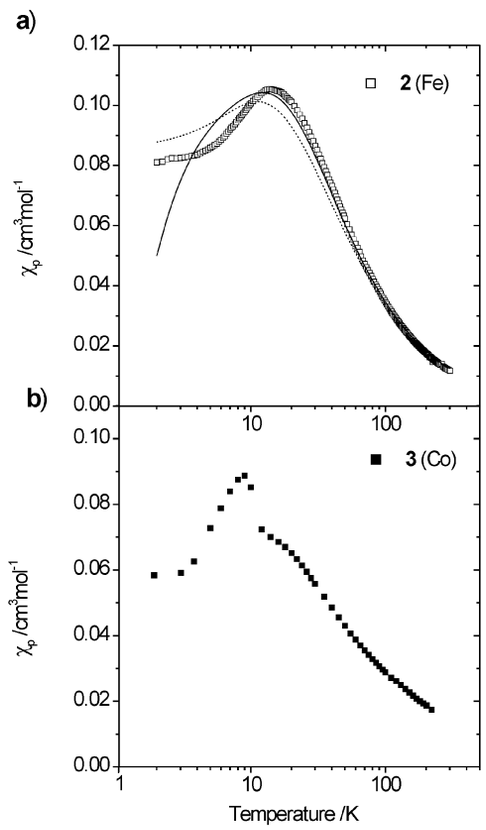

Fig. 4 (a) The magnetic susceptibility of **2** and the best fits for a simple $S = 2$ dimer model (solid line) and the $S = 2$ chain model (dashed line). (b) The magnetic susceptibility of **3** showing discontinuous behaviour at ~11 K indicative of a phase transition to a predominantly antiferromagnetic state.

Analysis of the magnetic lattice topology provides a model to fit the susceptibility data and therefore allow determination of the coupling constants. There are two important oxalate mediated superexchange pathways (described above). The first, J_1 is a consequence of the normal symmetric bridging mode that results in Δ,Λ-dimer formation with an Fe ··· Fe separation of 5.6624(16) Å (thick solid line in Fig. 2(a)) and the second, J_2, results from the asymmetric oxalate bridge (dashed line in Fig. 2(a)), with an Fe ··· Fe separation of 5.4955(11) Å. There is a third coupling pathway, $J_{interlayer}$, between iron atoms in adjacent layers. However the Fe ··· Fe separation is 6.216(18) Å, and the convoluted Fe–Cl ··· H–O–H ··· Cl–Fe pathway is expected to make this exchange coupling negligible. There are no simple analytical solutions for a realistic model comprised of the two couplings J_1 and J_2 connected in the network as shown in Fig. 2(b). In certain circumstances it may be valid to apply a simpler model. For instance if $|J_1| \gg |J_2|$ a simple $S = 2$ dimer model should reasonably describe the magnetism for $k_BT > |J_2|$. Alternatively if $|J_1| \ll |J_2|$ the network of J_2-couplings is a zigzag chain, and the data for $k_BT > |J_1|$ should

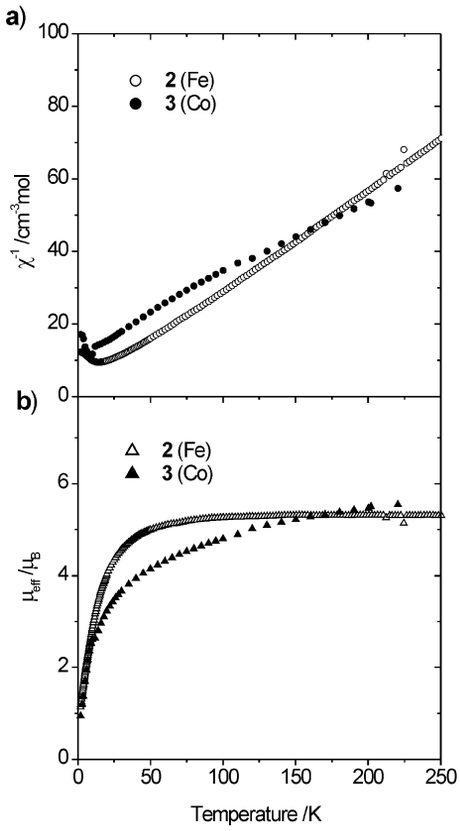

Fig. 5 (a) Plot of reciprocal susceptibility *vs.* temperature for **2** and **3**, showing the linear Curie–Weiss behaviour for the high-temperature data. (b) The thermal variation of the effective magnetic moments of **2** and **3**.

be modelled as a 1-D $S = 2$ system. For an intermediate situation with $|J_1| \sim |J_2|$, or when the thermal energy is comparable to the smallest coupling, neither of the models above is appropriate.

Fitting a simple isotropic dimer model[14] (eqn. (1)) to **2** (solid line in Fig. 4(a)) gives $J_1 = -1.96$ cm^{-1} and $g = 2.32$. This value of J agrees well with literature values of 2.5–3.3 cm^{-1} for symmetric oxalate bridged iron(II) dimers[3] and a value of 2.2 cm^{-1} determined for the mineral humboldtine.[15] The susceptibility of an antiferromagnetically coupled dimer must tend to zero at low temperatures whereas the susceptibility of **2** approaches 0.080 cm^3 mol^{-1}. The isotropic chain model (eqn. (2)) of classical $S = 2$ spin moments[16] gives a satisfactory fit only by constraining $g = 2.25$. This gives $J_2 = -1.89$ cm^{-1}. Allowing g to refine freely overestimates the high-temperature values of the susceptibility. Quantum calculations by Weng[17] for an $S = 2$ chain show that J_2 and g can be determined from T_{max} and $\chi(T_{max})$. We obtain $J_2 = -1.37$ cm^{-1} and a g-value of 2.43. The deviation of the data from both dimer and chain models, particularly at low temperatures suggests several possibilities: (a) both couplings J_1 and J_2 are significant, (b) isotropic models are insufficient and anisotropic terms must be considered, (c) the plate-like morphology of the crystallites results in an unavoidable partial alignment of the powder sample. Clearly a more sophisticated treatment is needed to determine the relative magnitudes of these couplings reliably.

$$\hat{\boldsymbol{H}} = -2J_1\boldsymbol{S}_1\cdot\boldsymbol{S}_2 \quad (1)$$

$$\hat{\boldsymbol{H}} = -2J_2\sum_i \boldsymbol{S}_i \cdot \boldsymbol{S}_{i+1} \quad (2)$$

The susceptibility of the cobalt derivative **3** increases on cooling, but shows signs of short-range order with a decrease in the rate of increase of $\chi(T)$ (Fig. 4(b)). At about 11 K there is a

discontinuity in the behaviour. Above 50 K this cobalt derivative obeys a Curie–Weiss law with $C = 5.10(5)$ cm^3 K mol^{-1} and $\theta = -74(2)$ K (Fig. 5). This corresponds to an effective room-temperature moment of 6.4 μ_B. For octahedrally coordinated cobalt(II) with a $^4T_{1g}$ ground term the observed moment is typically 4.7–5.2 μ_B. This anomalously large observed value may be due to magnetic anisotropy caused by the orbital contribution and a preferential alignment of the structurally anisotropic crystallites. The negative Weiss constant, the abruptness of the change in behaviour at 11 K, and the absence of a large spontaneous moment below this temperature, suggests a transition is to an antiferromagnetically ordered state. The absence of a broad maximum in **3** makes it impossible to obtain reliable coupling constants from the dimer and chain models. In this case the magnetic ordering transition suggests either the structure can be considered as a magnetically 3-D network (comprised of J_1, J_2 and $J_{interlayer}$), or that it can be thought of as a 2-D network (J_1 and J_2) with an Ising-like spin anisotropy.[18] Given the isostructural nature of these compounds it seems likely that single-ion anisotropy plays a key role in the formation of a magnetically ordered state.

Using hydrothermal conditions we have been able to form a new stable complex metal oxalate network structure. The limited solubility of its constituents under ambient conditions means that this phase is only accessible by hydrothermal methods. The isostructural nature of these derivatives allows us to clearly see the effects of CFSE on the metal coordination sphere one electron at a time. Furthermore the dramatic differences in the low-temperature magnetic behaviour of **2** and **3** are attributable to the change in single ion anisotropy of the metal ions caused by the changing electronic configuration.

Acknowledgements

The authors gratefully acknowledged the EPSRC of the United Kingdom for financial support.

References

1 R. Vaidhyanathan, S. Natarajan and C. N. R. Rao, *Inorg. Chem.*, 2002, **41**, 4496; R. Vaidhyanathan, S. Natarajan and C. N. R. Rao, *Solid State Sci.*, 2002, **4**, 633; R. Vaidhyanathan, S. Natarajan and C. N. R. Rao, *J. Solid State Chem.*, 2001, **162**, 150; R. Vaidhyanathan, S. Natarajan and C. N. R. Rao, *Chem. Mater.*, 2001, **13**, 185; R. Vaidhyanathan, S. Natarajan and C. N. R. Rao, *J. Chem. Soc., Dalton Trans.*, 2001, 699.
2 S. Natarajan, R. Vaidhyanathan, C. N. R. Rao, S. Ayyappan and A. K. Cheetham, *Chem. Mater.*, 1999, **11**, 1633; R. Vaidhyanathan, S. Natarajan, A. K. Cheetham and C. N. R. Rao, *Chem. Mater.*, 1999, **11**, 3636; S. Ayyappan, A. K. Cheetham, S. Natarajan and C. N. R. Rao, *Chem. Mater.*, 1998, **10**, 3746.
3 J. Gelrup, P. A. Goodson, D. J. Hodgson and K. Michelsen, *Inorg. Chem.*, 1995, **34**, 6255.
4 F. Mazzi and G. Garavelli, *Period. Mineral.*, 1957, **26**, 269; R. Deyrieux and A. Peneloux, *Bull. Soc. Chim. Fr.*, 1969, **8**, 2675.
5 D. Visser, S. G. Carling, I. D. Watts, P. Day and K. H. Andersen, *Physica B*, 1999, **267–268**, 266; S. G. Carling and P. Day, *Polyhedron*, 2001, **20**, 1525; I. D. Watts, S. G. Carling and P. Day, *J. Chem. Soc., Dalton Trans.*, 2002, 1429; C. J. Nuttall, S. G. Carling and P. Day, *Mol. Cryst. Liq., Cryst., Sect. A*, 1999, **334**, 615.
6 S. Decurtins, R. Pellaux, G. Antorrena and F. Palacio, *Coord. Chem. Rev.*, 1999, **192**, 841; S. Decurtins, H. W. Schmalle, R. Pellaux, P. Schneuwly and A. Hauser, *Inorg. Chem.*, 1996, **35**, 1451; S. Decurtins, H. W. Schmalle, P. Schneuwly, J. Ensling and P. Gütlich, *J. Am. Chem. Soc.*, 1994, **116**, 9521; S. Decurtins, H. W. Schmalle, P. Schneuwly and H. R. Oswald, *Inorg. Chem.*, 1993, **32**, 1888.
7 See, for example: O. Kahn, *Molecular Magnetism*, VCH, Weinheim, 1993.
8 Z. Otwinowski and W. Minor, *Methods Enzymol.*, 1997, **276**, 307–326.
9 G. M. Sheldrick, SHELXL97 and SHELXS97: University of Göttingen, Germany, 1997.
10 S. T. Bowden, *The Phase Rule and Phase Reactions*, Macmillan and Co. Ltd., London, 1954.
11 D. J. Price, A. K. Powell and P. T. Wood, *J. Chem. Soc., Dalton Trans.*, 2000, 3566.
12 H. Siems and J. Löhn, *Z. Anorg. Allg. Chem.*, 1972, **393**, 97.
13 M. C. Etter, J. C. MacDonald and J. Bernstein, *Acta Crystallogr., Sect. B*, 1990, **46**, 256.
14 C. J. O'Conner, *Prog. Inorg. Chem.*, 1982, **29**, 203.
15 I. Sledzinska, A. Murasik and M. Piotrowski, *Physica B*, 1986, **138**, 315.
16 M. E. Fisher, *Am. J. Phys.*, 1964, **32**, 343.
17 C. Y. Weng, Ph. D. Thesis, Carnegie–Mellon University, Pittsburgh, PA, 1969; see also: W. Hiller, J. Strähle, A. Datz, M. Hanack, W. E. Hatfield, L. E. ter Haar and P. Gütlich, *J. Am. Chem. Soc.*, 1984, **106**, 329.
18 See, for example: F. Palacio, in *Molecular Magnetism: From Molecular Assemblies to the Devices*, ed. E. Coronado, P. Delhaés, D. Gatteshi and J. S. Miller, NATO ASI series E: Applied Sciences, Kluwer Academic Publishers, Dordrecht, 1996, vol. 321, pp. 5–64.